Proceedings of the 16th International Conference on Nuclear Engineering
ICONE16
May 11-15, 2008, Orlando, Florida, USA

ICONE16-48077

SWIRLING ANNULAR FLOW IN A STEAM SEPARATOR

Hironobu Kataoka **Akira Sou** **Shigeo Hosokawa** **Akio Tomiyama**
Graduate School of Engineering, Kobe University
Rokkodai, Nada, Kobe 657-8501, Japan

ABSTRACT

Effects of pick-off ring configuration on the separation performance of a downscaled model of a steam separator for a boiling water nuclear reactor are examined using various types of pick-off rings. The experiments are conducted using air and water. Pressure drops in a barrel and a diffuser, and diameters and velocities of droplets at the exit of the barrel are measured using differential pressure transducers and particle doppler anemometry, respectively. As a result, the following conclusions are obtained: (1) the separation performance does not depend on the shape of pick-off ring, but strongly depends on the width of the gap between the pick-off ring and the barrel wall, (2) the pressure drop in the barrel is well evaluated using the interfacial friction factor for unstable film flows, and (3) the radial distribution of droplet velocity at the exit of the separator is of use for the evaluation of carry-under.

INTRODUCTION

Boiling water nuclear reactors, BWR, are equipped with steam separators for splitting a two-phase mixture into steam and water before feeding steam to dryers and turbines. The steam separator consists of a standpipe, a diffuser with a swirler, and a barrel with several pick-off-rings (POR). Stationary vanes of the swirler apply a large centrifugal force to the flow, and thereby, most of water rapidly migrates toward the barrel wall. An annular swirling flow with few droplets in the gas core is, therefore, formed in the barrel. The liquid film flow is removed by the PORs from the gas core flow. However we have little knowledge on the annular swirling flow in the separator.

In our previous study [1,2], flow patterns, liquid film thickness, the ratio of the separated film flow rate to the total liquid flow rate in air-water annular swirling flows in a one-fifth scale model of the steam separator were, therefore, measured to understand characteristics of the swirling flow and to establish an experimental database applicable to the modeling and verification of numerical methods for predicting the two-phase flow in the steam separator.

In the present study, the effects of POR configuration on the separation performance are examined by carrying out experiments using various PORs. Pressure drops in the barrel and the diffuser are measured and compared with available correlations. Velocities and diameters of droplets at the exit of the separator are also measured. Droplet velocities are utilized to evaluate the carry-under of the gas phase flowing into the separated flow and the carry-over of non-separated liquid.

EXPERIMENTAL SETUP

Figure 1 shows the experimental apparatus. It consisted of the upper tank, the barrel, the diffuser, the standpipe, the plenum, the gas-liquid mixing section, the water supply system and the air supply system. The barrel, the diffuser and the standpipe were made of transparent acrylic resin for observation and optical measurements of two-phase flows. The size was one-fifth of the actual steam separator used in BWR. Air was supplied from the oil-free compressor (Oil-free Scroll 11, Hitachi Ltd.), the regulator (R600-20, CKD) and the flowmeter (FLT-N, Flowcell, Ltd.) to the mixing section. Tap water at room temperature (20 ^{o}C) was supplied from the magnet pump (MD-40RX Iwaki, Ltd.) and the flowmeter to the mixing section. The two-phase flow formed in the mixing section flowed up through the plenum of 60 mm in inner diameter D and 300 mm in length L, the standpipe of D = 30 mm and L = 200 mm, the diffuser of L = 33 mm and the barrel of D = 40 mm and L = 270 mm.

The swirler shown in **Fig. 2**, which was made of ABS resin, was installed in the diffuser to form a swirling flow in the barrel. Its shape was based on an actual swirler. Experiments without the swirler were also conducted to examine its effects on pressure drop and the separator performance. As will be discussed later, most of flow patterns observed in the barrel were annular flows consisting of liquid film flow, gas flow and droplet flow.

Figure 3 shows the upper part of the barrel, the upper tank and the device for separating the film flow from the gas core flow, i.e. the mixture of gas and droplet flows. In an actual steam separator, the so-called pick-off-ring, POR, is utilized for the separation. An inner pipe was inserted in the barrel to simulate POR. The lower end of the inner pipe located 220 mm above the bottom of the barrel.

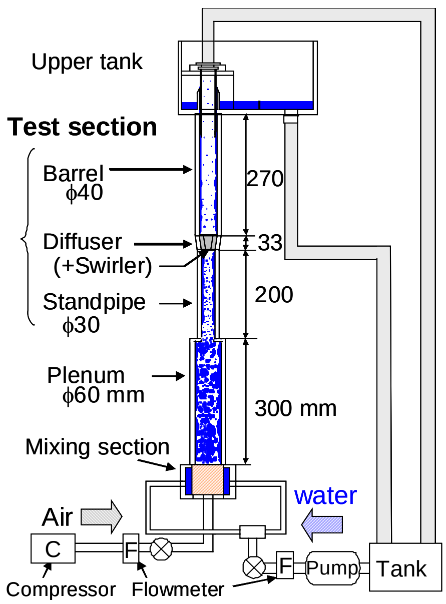

Fig. 1 Experimental apparatus

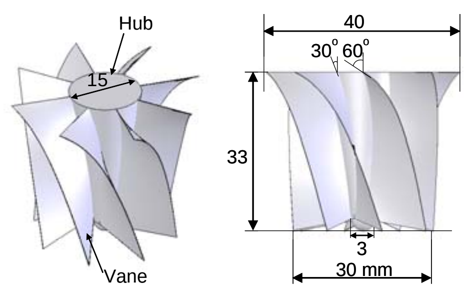

(a) bird's-eye view (b) side view

Fig. 2 Swirler with a hub and stationary vanes

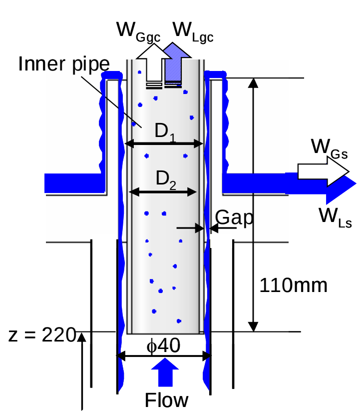

Fig. 3 Pick-Off-Ring (POR)

Table 1 Specifications of pick-off rings

Type	b_{Gap} (mm)	T (mm)	Shape	D_1 (mm)	D_2 (mm)
1	2	2	Flat	36	32
2	2	1	Flat	36	34
3	2	0.5	Flat	36	35
4	2	2	Taper	36	32
5	4	2	Taper	32	28

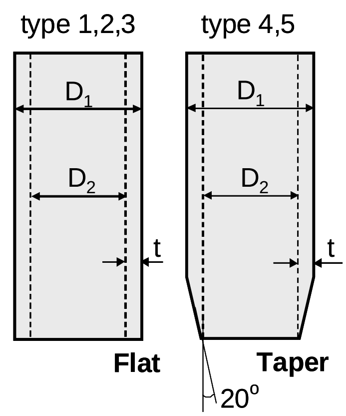

Fig. 4 POR shapes

Five types of inner pipes listed in **Table 1** were used to study the effects of POR configuration (See **Fig. 4**) on the separation performance. Most of the liquid film flowed through the gap between the barrel wall and the outer wall of the inner pipe, while most of air and droplets flowed through the inner pipe. The separated liquid and the droplets carried over returned to the water reservoir through independent pipelines.

Experimental conditions were determined by adjusting the values of the flow quality and the two-phase centrifugal force to cover those in the nominal operating condition of the BWR separator. The values of the quality x, the gas and liquid volume fluxes J_G and J_L corresponding to the nominal operating condition were x = 0.18, J_G =14.6 m/s and J_L =0.08 m/s, respectively [1].

The mass flow rates W_{Ls} and W_{Lgc} of the separated liquid and liquids in the gas core returning to the reservoir were measured using a timer and a graduated cylinder. Each measurement was conducted for 50 seconds to make the uncertainty in measured W less than 3 %. The ratio W_s^* of the separated flow to the total liquid flow rate defined by

$$W_s{*} = \frac{W_{Ls}}{W_{Ls} + W_{Lgc}} \qquad (1)$$

was used as an index of the separator performance.

The film thickness δ was measured using a laser focus displacement meter (LFD, LT-9030, Keyence, Ltd.) [3]. The sampling period was 0.64 ms and the measurement time was 30 seconds. The sampling number was, therefore, more than 46000 points, the number of which was sufficient to obtain accurate time-averaged film thicknesses. The uncertainty in measured δ was 2.0 %.

Pressure drops in the diffuser and the barrel were measured using differential pressure transducers (DP45, Valydine). As shown in **Fig. 5**, six holes of 1 mm in diameter were made at six elevations to measure pressure drops between two elevations. The sampling period was 0.64 ms and the measurement time was 30 seconds, which was long enough to obtain accurate time-averaged pressure drops. The uncertainty in measured pressure drop was less than 0.5%.

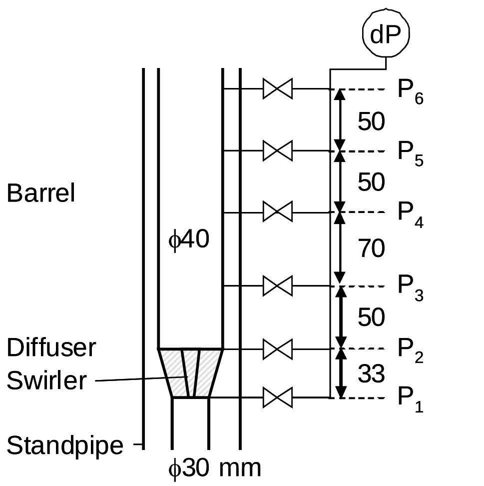

Fig. 5 Pressure drop measurement

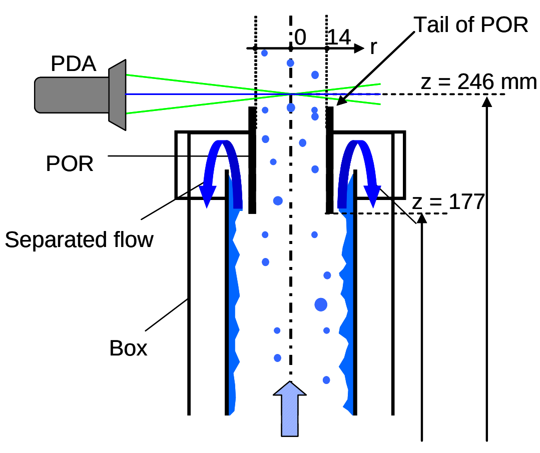

Fig. 6 Liquid film separation device for PDA

As shown in **Fig. 6**, a device for separating the liquid film flow from the gas core flow was installed on top of the shortened barrel in the case of measuring diameters and velocities of droplets in the gas core flow using a Particle Doppler Anemometry (PDA) system (58N series, DANTEC). The device was equipped with a POR whose gap b_{Gap} between the outer surface of the POR and the inter surface of the barrel, thickness t and inner diameter D_2 were 4, 2 and 28 mm, respectively. Droplet diameters and velocities were measured at 246 mm downstream of the swirler. The uncertainties in measured diameters and velocities of droplets were less than 1 % and 0.5 %, respectively.

Flow patterns in the barrel and standpipe were recorded using a high-speed video camera (Redlake Motion Pro HS-1, frame rate = 2000 – 2500 fps, exposure time = 100 μs).

RESULTS AND DISCUSSION

Flow pattern

Images of annular flow patterns without and with the swirler are shown in **Figs. 7 (a) and (b)**, respectively. Without the swirler, the droplet deposition takes place all over the barrel. In the case of swirling flow, the rotational speed of the flow increases with J_G, and as shown in Fig. 7 (b) spiral streaks are formed from the swirler vanes in the annular flow condition. Most of the liquid in the streak might be made of liquid deposited on the swirler vanes, that is, the liquid transfer from droplets to the film is caused not only by the direct droplet deposition but also by the collection of droplets and film on the vanes [4]. As for the direct deposition, most of droplets deposit on the liquid film within a short distance from the swirler (about 150 mm) due to a large centrifugal force generated by the swirling flow. This, in turn, implies that few droplets remain in the gas core flow in far downstream of the swirler.

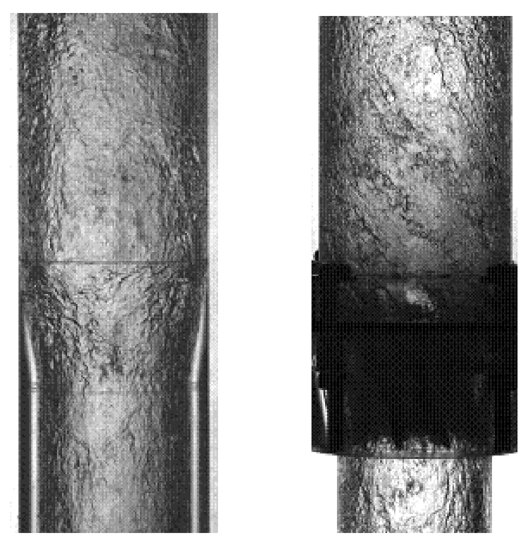

(a) without a swirler (b) with a swirler

Fig. 7 Annular flow in diffuser and barrel (J_G = 14.6 m/s, J_L = 0.08 m/s)

Film thickness

Mean film thicknesses δ_{avg} at 170 mm above the swirler are shown in **Fig. 8**, which clearly shows that δ_{avg} in swirling flows takes a higher value and depends more strongly on J_L than in non-swirling flows. The strong dependence on J_L is in accordance with the fact that the film flow rate is close to the total liquid flow rate in swirling flows, i.e., the increase in J_L

directly reflects the increase in the film flow rate. On the other hand, the droplet flow rate in non-swirling flows increases with J_L, and therefore, δ_{avg} does not depend on J_L so much in non-swirling flows. As shown in **Fig. 9**, the maximum film thickness δ_{max} is slightly higher in swirling flows than in non-swirling flows, and is about three times as large as δ_{avg}. It should be noted that δ_{max} is larger than b_{Gap} of type 1-4 PORs (=2 mm) at low J_G.

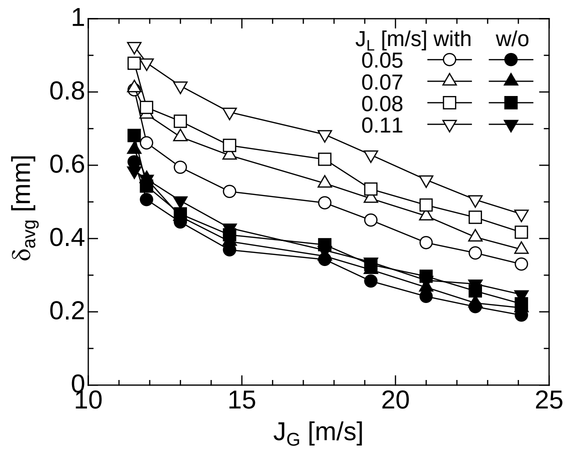

Fig. 8 Effects of J_G and J_L on δ_{avg} (z = 170 mm)

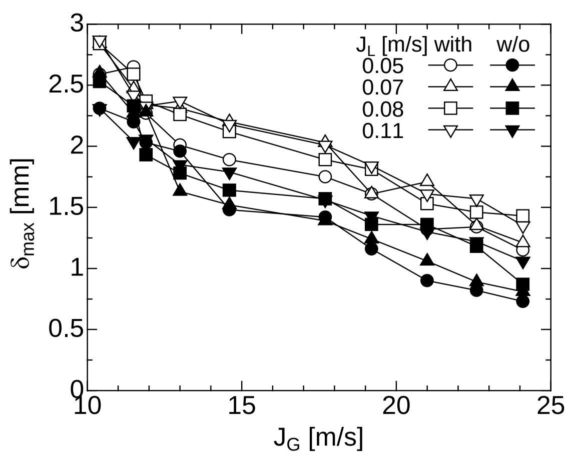

Fig. 9 Effects of J_G and J_L on δ_{max} (z = 170 mm)

Flow Separation

Figure 10 shows W_s^* for swirling and non-swirling flows measured by using type 4 POR (gap size b_{Gap} = 2 mm, POR thickness t = 2 mm). The W_s^* with the swirler is larger than that without it, which implies that the swirler is an effective device for the flow separation. The effects are marked under annular flow conditions (J_G > 13 m/s). Without the swirler, W_s^* increases with J_G in churn flow, while it decreases with increasing J_G in annular flow due to the enhancement of droplet entrainment at high J_G. In annular swirling flow W_s^* increases with J_G. This is due to the increase in the liquid film flow rate resulting from the large deposition rate caused by the strong centrifugal force.

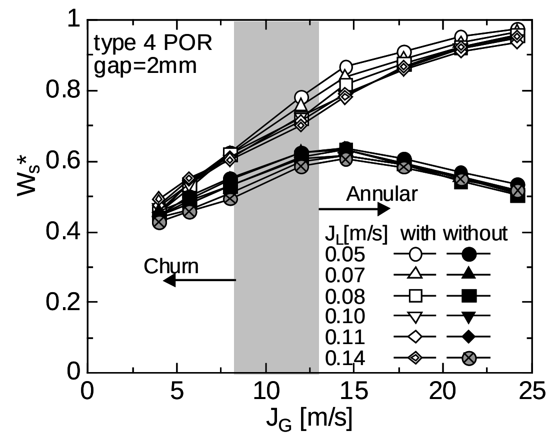

Fig. 10 Effects of swirler on W_s*.

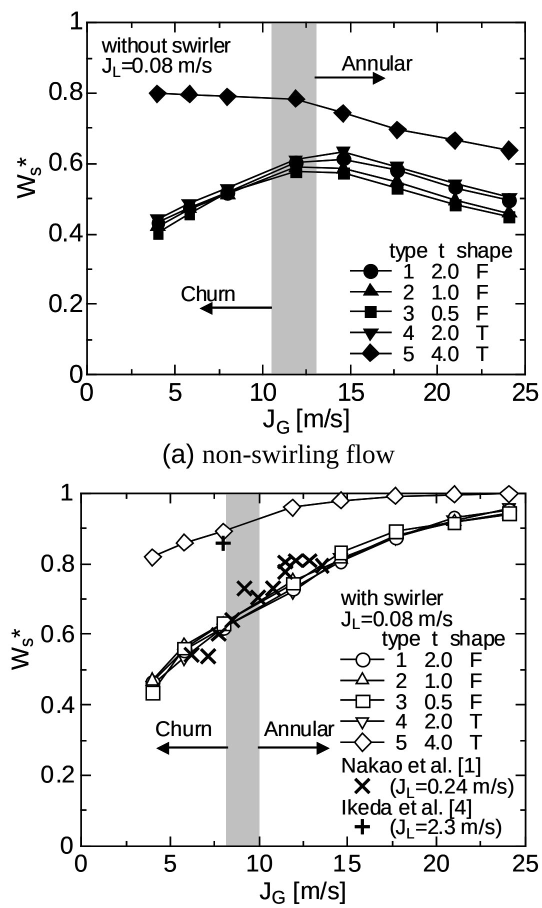

(a) non-swirling flow

(b) swirling flow

Fig. 11 Effects of POR shape on W_s*.

The effects of POR configuration on W_s^* is shown in **Fig. 11**. Experimental data obtained by Nakao et al. and Ikeda et al. are also plotted in Fig. 11 (b). Their data show a similar trend with the present data. Although the dimensions of the experimental apparatus used in their studies are not clear, they were based on the steam separators. Hence, the agreement implies the validity of the present separator model. The W_s* of type 5 POR (gap size b_{Gap} = 4 mm) is larger than that of the other PORs of 2 mm gap, which implies the existence of liquids in the region between 2 and 4mm from the inner wall. On the other hand, in the cases of 2 mm gap (type 1-4) the effects of POR configuration under churn flow conditions are negligible since the maximum film thickness is larger than b_{Gap} [8] and separated liquid flow rate W_s must be determined by the pressure drop in the gap. The W_s* for annular non-swirling flow is affected by POR shape, that is, W_s* takes a larger value with the tapered POR or with thicker PORs since the droplet flow rate in the POR gap is large in these cases. The W_s* is not affected by POR shape for swirling flow because the droplet flow rate is reduced by a large centrifugal force. These results imply that POR configuration cannot be determined without taking into account liquid film thickness.

Pressure drop

Figure 12 shows pressure gradients –dP/dz in the diffuser and barrel. As shown in Fig. 12 (a), pressure recovery due to deceleration increases with J_G. On the other hand, –dP/dz in swirling flows is larger than that in non-swirling flows since the swirler causes a singular pressure drop. In non-swirling flow, the region of the pressure recovery extends downstream of the diffuser as J_G increases. This must be due to the enlargement of the region of a separated recirculating flow. As shown in Fig. 12, the swirler increases the pressure drop in the barrel especially near the swirler, and the pressure drop near the swirler increases with J_G. These increases may be caused by a large centrifugal force, a strong interfacial shear stress acting on the film surface roughened by the spiral streaks, and an enhanced droplet deposition. Axial pressure distributions are shown in **Fig. 13**. The pressure drop is large in the diffuser and within 100 mm from the swirler where the swirling flow is strong, the spiral streaks appear from the vanes, and droplet deposition is enhanced.

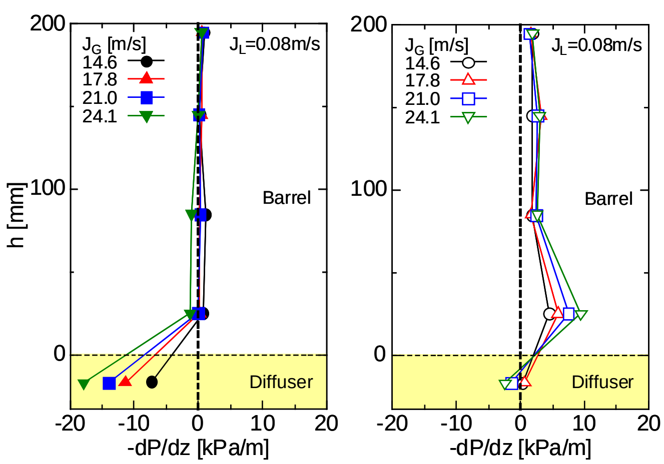

(a) Without swirler (b) With swirler

Fig. 12 Pressure gradient

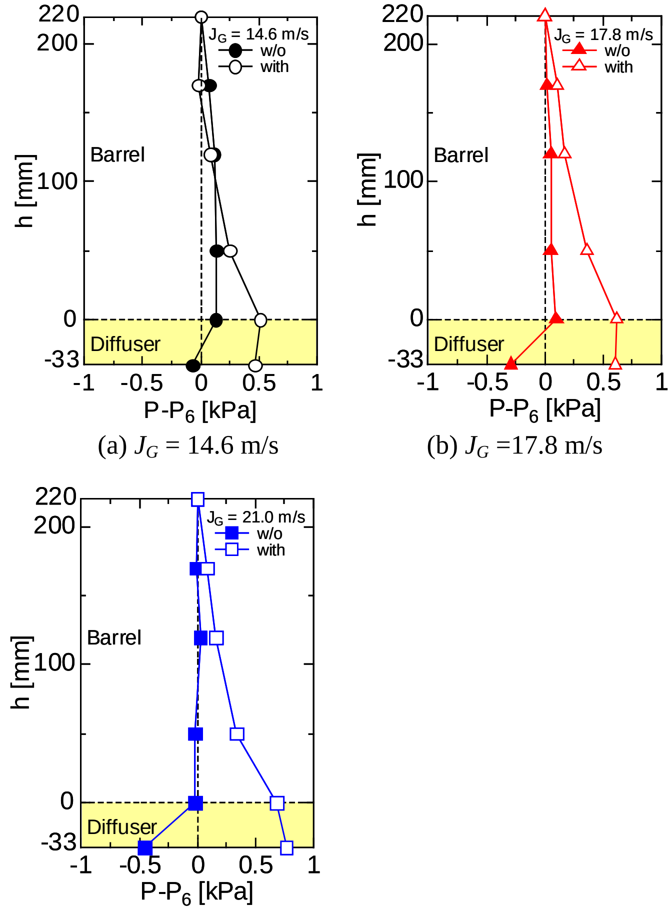

(a) J_G = 14.6 m/s (b) J_G =17.8 m/s

(c) J_G = 21.0 m/s

Fig. 13 Pressure distribution

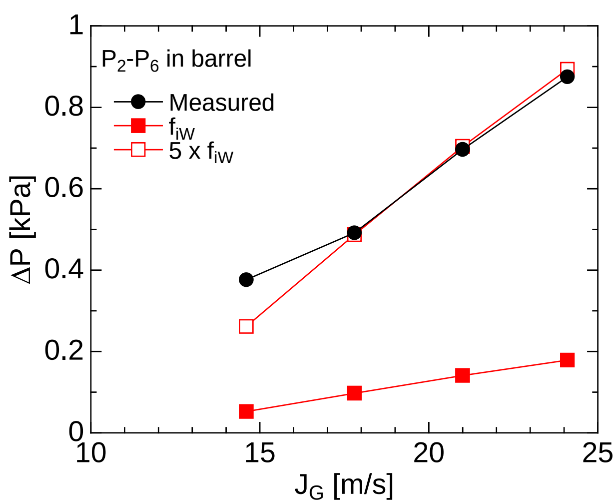

Fig. 14 Pressure drops of swirling flows in the barrel

Pressure drops can be estimated as the sum of the frictional and static pressure drops:

$$\Delta P = \frac{4}{D}\tau_w \Delta z + \rho_m g \Delta z \tag{2}$$

where τ_w is the wall shear stress, Δz the axial distance, ρ_m the mixture density, and g the acceleration of gravity. Since the droplet volume fraction in swirling flow is negligible, ρ_m is estimated by

$$\rho_m = \rho_G(1-\alpha_F) + \rho_F \alpha_F \tag{3}$$

Here α is the volume fraction, ρ the density, the subscripts G and F denote the gas and liquid film, respectively. The film volume fraction is given by

$$\alpha_F = 4A_F/(\pi D^2) \tag{4}$$

where

$$A_F = \pi\delta_{avg}(D-\delta_{avg}) \tag{5}$$

The balance of the forces acting on the film flow yields

$$\tau_w = \tau_i - \rho_L g \delta_{avg} \tag{6}$$

where τ_i is the interfacial shear stress acting on the liquid film:

$$\tau_i = f_i \frac{1}{2}\rho_G V_G^2 \tag{7}$$

where f_i is the interfacial friction factor and V_G the gas velocity. For stable films, f_i can be evaluated by the Wallis correlation[5]:

$$f_{iW} = 0.005(1+300\frac{\delta_{avg}}{D}) \tag{8}$$

For unstable films, f_i is known to be well evaluated by [6]

$$f_{iU} = \max\{5 f_{iW},\ f_{iH}\} \tag{9}$$

where f_{iH} is the friction factor proposed by Henstock & Hanratty [7]. Note that $5f_{iW} > f_{iH}$ in the present experimental conditions, and therefore, f_{iU} is equal to $5f_{iW}$.

Pressure drops ΔP (= $P_2 - P_6$) of annular swirling flows in the barrel are shown in **Fig. 14**. The Wallis correlation, Eq.(8), for stable films underestimates ΔP, whereas $5f_{iW}$ for unstable films agrees well with the measured ΔP. This implies that the film flow in swirling flow is highly agitated to be regarded as an unstable film.

Droplet diameter and velocity

Front views of gas core flows discharged from the film separation device are shown in **Fig. 15**. A number of droplets are observed in non-swirling flows, whereas the number density of droplets is much smaller in swirling flows.

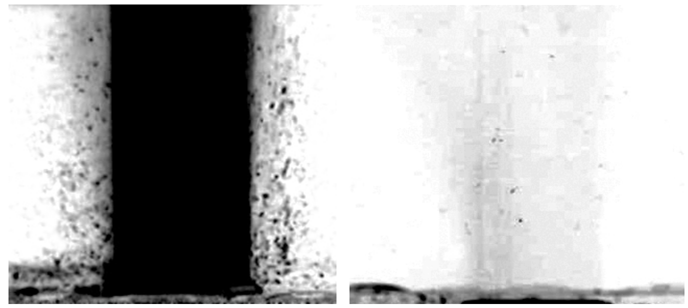

(a) non-swirling flow (b) swirling flow

Fig. 15 Gas core flows at the exit of the barrel

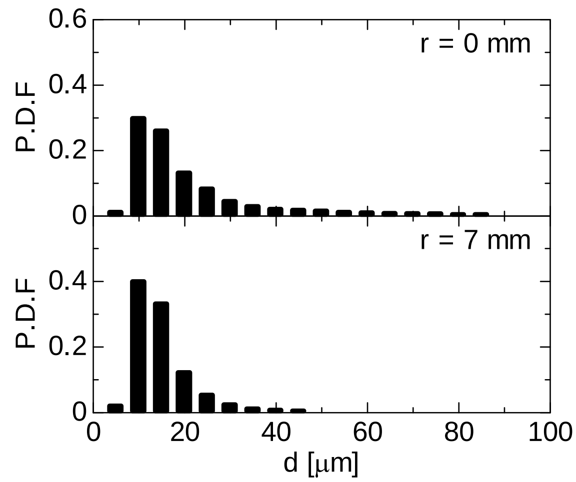

Fig. 16 Distribution of droplet diameter in swirling flow (z = 246 mm, J_G = 14.6 m/s, J_L = 0.08 m/s)

PDA measurement was carried out for swirling flows. Though the measurement was done for $0 \leq r \leq 14$ mm (the definition of radial coordinate r is shown in Fig. 6), the accuracy of measured droplet diameter for $r > 8$ mm is low because of the presence of large droplets formed by the breakup of thin films at the tail of POR.

Figure 16 shows distributions of droplet diameter for J_G = 14.6 m/s and J_L = 0.08 m/s measured at the barrel center (r = 0 mm, z = 246 mm) and in the middle (r = 7 mm, z = 246 mm). Since the centrifugal force F_c acting on a droplet is proportional to its mass and r, the P.D.F. of droplets larger than 10 μm decreases with increasing r due to the increase in F_c, and some of large droplets (droplet diameter d > 40 μm) remain at the center because $F_c = 0$ at $r = 0$.

Figures 17 (a) and (b) show effects of J_L and J_G on the Sauter mean diameter d_{32}, respectively. Here d_{32} is defined by

$$d_{32} = \sum_{i=1}^{N} d_i^3 \Big/ \sum_{i=1}^{N} d_i^2 \tag{10}$$

where d_i is the diameter of the i-th droplet, and N the total number of droplets. The d_{32} is smaller than 70 μm and is not affected by J_L. On the other hand, it decreases with increasing J_G due to the increase in the centrifugal force.

Radial distributions of mean streamwise velocity V_D of droplets in swirling flows are shown in **Fig. 18**. The broken line in Fig. 18 (a) is the one-seventh power law based on the assumption of no carry-under and no carry-over. Although V_D shows a similar trend to the power law, the former is smaller than the latter due to carry-under. The V_D increases with J_L, which is caused by the decrease in carry-under due to the increase in film thickness at larger J_L. Since the droplet slip velocity is negligible (about 0.05 m/s), V_D is approximately equal to the gas velocity. Hence the increase rate of V_D is proportional to that of J_G as can be understood from Fig. 18 (b).

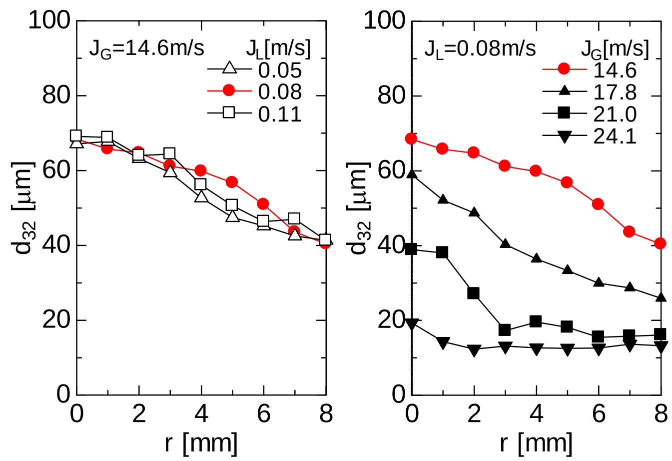

(a) Influence of J_L (b) Influence of J_G

Fig. 17 Sauter mean diameter d_{32}

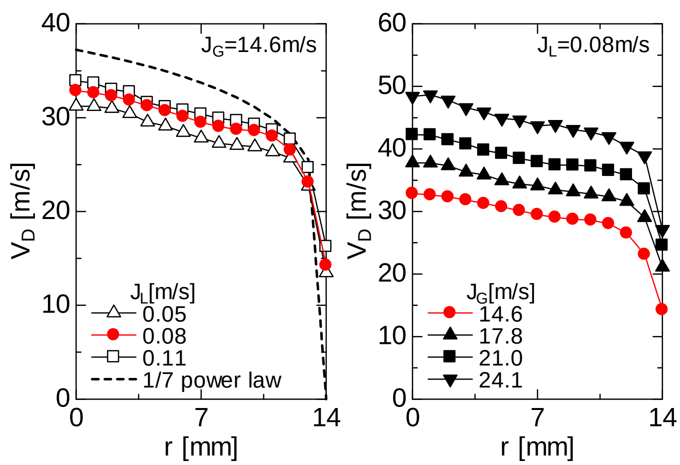

(a) Influence of J_L (b) Influence of J_G

Fig. 18 Mean vertical velocity V_D of droplets

Evaluation of carry-under and carry-over

The carry-under CU is defined by

$$CU = \frac{W_{Gs}}{W_{Gs} + W_{Ls}} \tag{11}$$

where W_{Gs} is the mass flow rate of the separated gas. It is not easy to measure CU because of the difficulty in measuring W_{Gs}. The separated gas flow rate *is* given by

$$W_{Gs} = W_G - W_{Ggc} \tag{12}$$

where W_G is the total mass flow rate of the gas and W_{Ggc} the mass flow rate of the gas in the gas core. The droplet velocity V_D is close to V_G and the droplet volume fraction α_D is negligible. Hence W_{Ggc} is estimated by

$$W_{Ggc} = \rho_G \int_0^{D/2} V_D 2\pi r\, dr \tag{13}$$

Equations (11), (12) and (13) can be utilized to estimate CU.

The carry-over CO is defined by

$$CO = \frac{W_{Lgc}}{W_{Ggc} + W_{Lgc}} \tag{14}$$

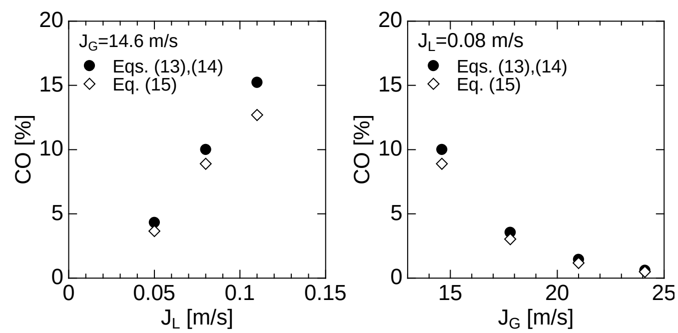

(a) Carry-over

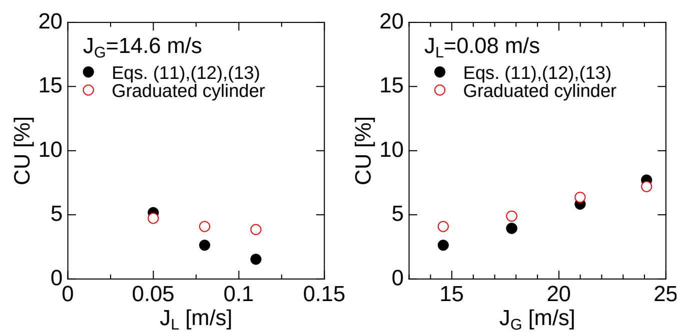

(b) Carry-under

Fig. 19 Carry-over CO and carry-under CU

Instead of using W_{Ggc}, CO can be estimated by

$$CO \cong \frac{W_{Lgc}}{W_G + W_{Lgc}} \tag{15}$$

because $W_{Ggc}+W_{Lgc} \simeq W_G+W_{Lgc}$.

Figures 19 (a) and (b) are CO and CU of type 5 POR, respectively. As expected, Eq.(15) gives slightly smaller values CO than Eqs.(13) and (14), so that Eq.(15) can be also utilized to evaluate CO. The decreases in J_L or increase in J_G causes the decrease in the film thickness, which, in turn, increases CU. This tendency is well captured in the measured CU. As shown in Fig. 19 (b), CU was also measured by using a graduated cylinder and a timer, though there might be non-negligible errors in this measurement. In any case, CU measured by the two methods agreed well, by which we could confirm that the drop velocity is useful for evaluating CU.

CONCLUSION

The effects of pick-off ring (POR) configuration on the separation performance of a downscaled model of a steam separator for a boiling water nuclear reactor are examined using various types of PORs. The experiments are conducted using air and water. Pressure drops in a barrel and a diffuser are measured using differential pressure transducers. Droplet velocities are measured using a Particle Doppler Anemometry (PDA) system, which are utilized to evaluate carry-under and carry-over. As a result, the following conclusions are obtained.

(1) The separation performance does not depend on the shape and thickness of POR, but strongly depends on the gap width.

(2) The pressure drop in the barrel is well predicted by using the interfacial friction factor, $5f_{wi}$, where f_{wi} is the Wallis correlation of the interfacial friction factor for annular flow with stable film.

(3) The carry-under and carry-over are well estimated by making use of the radial distribution of droplet velocity at the exit of the separator.

ACKNOWLEDGMENTS

The authors gratefully acknowledge the financial support by "Innovation and Viable Nuclear Energy Technology Development Project", Ministry of Economy, Trade and Industry, Japan, and the assistance in experiments by Mr. D. Nishiwaki and Mr. Y. Shinkai.

REFERENCES

[1] Kataoka, H., Tomiyama, A., Hosokawa, S., Sou, A. and Chaki, M., Two-Phase Swirling Flow in a Gas-Liquid Separator, J. Power and Energy Systems, (2007) submitted

[2] Kataoka, H., Tomiyama, A., Hosokawa, S., Sou, A. and Chaki, M., Effects of Pick-Off-Ring Configuration on Separation Performance of a Gas-Liquid Separator, Progress in Multiphase Flow Research, (2007) submitted

[3] Takamasa, T. and Hazuku, T., Measuring a Film Flowing Down a Vertical Wall Using Laser Focus Displacement Meters (1st Rep.), Trans. Japan Soc. Mech. Eng., Ser. B, Vol. 64, No. 617, pp.128-135, in Japanese, (1998)

[4] Hills, J. H., Azzopardi, B. J. and Barhey, A. S., Spatial Unsteadiness -A Way Towards Intensive Gas-Liquid Reactors-, Trans. Inst. Chem. Eng., Vol. 74, Part A, pp. 567-574, (1996)

[5] Wallis, G. B., One Dimensional Two-Phase Flow, McGraw-Hill, pp. 318-322, (1969)

[6] Thurgood, M. J., Kelly, J. M., Guidotti, T. E., Kohrt, R. J. and Crowell, K. R., COBRA/TRAC -A Thermal-Hydraulics Code for Transient Analysis of Nuclear Reactor Vessels and Primary Coolant Systems- Volume 1: Equations and Constitutive Models, NUREG/CR-3046, PNL-4385, Vol. 1, pp. 3.22-28 (1983)

[7] Henstock, W. H. and Hanratty, T. J., The Interfacial Drag and the Height of the Wall Layer in Annular Flows, AIChE J., 22, pp. 990-1000, (1976).